Journal of Polymer Research (2023) 30:189
https://doi.org/10.1007/s10965-023-03566-0

ORIGINAL PAPER

Synthesis and characterization of Chitosan-Avocado seed starch hydrogels as electrolytes for zinc-air batteries

María I. Cruz-Balaz[1] · María Fernanda Bósquez-Cáceres[1] · José Béjar[2] · Lorena Álvarez-Contreras[2] · Vivian Morera Córdova[1] · Juan P. Tafur[1]

Received: 5 February 2023 / Accepted: 18 April 2023 / Published online: 8 May 2023

Abstract
The application of innovative batteries is considered a plausible option to overcome the need to store energy. Current investigations focus on improving electrolytes in solid or gel states. Biopolymers are an excellent choice for gel electrolytes. In addition, polymer blends offer a high amorphous system compared to a single polymer improving its properties. In the present work, gel polymeric electrolytes (GPEs) were synthesized based on chitosan and starch. Chitosan and starch are compatible, and they served as a polymer host due to their high structural strength and low crystallinity degree. Moreover, epichlorohydrin was employed as a chemical crosslinker to create a reasonable degree of swelling of 12 M KOH solution. Hydrogels of different compositions were structurally and electrochemically characterized by ATR-Fourier Infrared Spectroscopy (ATR-FTIR), X-Ray Diffraction (XRD), Thermogravimetric Analysis (TGA), Scanning Electron Microscopy (SEM) and Cyclic Voltammetry (CV). The electrolyte film with the highest conductivity values was CS:A 3:3 embedded in 12 M KOH solution, which reached a conductivity of 0.027 $S{\cdot}cm^{-1}$ at room temperature. Structural characterization of chitosan-starch membranes showed an enhanced thermal stability and decrease in crystallinity degree due to the reticulation and absorption of KOH. The cyclic voltammetry study showed a quasi-reversible behavior of the GPEs during the redox processes. Finally, GPEs were tested in Zn-air batteries, with a maximum power density of 8.82 $mW{\cdot}cm^{-2}$ for CS:A 3:3 Sw at 25 °C. The present study suggests that chitosan-starch GPEs can be good candidates to support the sustainable energy transition.

Keywords Avocado starch · Polymeric electrolytes · Hydrogels · Zinc batteries

Introduction

Polymer electrolytes (PEs) are membranes that allow ion transport from the anode to the cathode and prevent electron flow between them. PEs are considered a possible ionically active material since the discovery of poly(ethylene oxide) (PEO) complexes doped with alkali metal ions by Fenton and Parker [1]. Furthermore, its possible application in energy devices was proposed by Armand [2]. PEs have attracted attention as a safer choice than liquid electrolytes [3]. The main disadvantage is the low ionic conductivities at room temperature [4, 5]. An option to solve this drawback is the use of gel polymer electrolytes (GPEs). They may be neither liquid nor solid, which confers the advantages of the ion diffusive properties of liquids and the cohesive behavior of solids [6]. GPEs can be applied in energy storage devices such as metal-air batteries. Nevertheless, they must fulfill high ionic conductivities, good mechanical and electrochemical properties at a wide temperature range [7].

Metal-air batteries are considered an efficient alternative to replace fossil fuels and for net zero emissions as the next generation of electrochemical energy storage, essentially due to the high theoretical energy densities and free air source for the cathode [8]. Among several metals, special attention has been given to Zn because it is less reactive than Li; additionally, Zn is the fourth most abundant element in the earth's crust (300 times more than Li), which translates into cost reduction [9]. Zinc-air batteries (ZABs) convert chemical energy into electrical energy and vice versa during

✉ Juan P. Tafur
jtafur@yachaytech.edu.ec

[1] Grupo de Investigación Aplicada en Materiales y Procesos (GIAMP), School of Chemical Sciences & Engineering, Yachay Tech University, Urcuquí 100115, Ecuador

[2] Centro de Investigación en Materiales Avanzados S.C. (CIMAV), Miguel de Cervantes No. 120, Complejo Industrial Chihuahua, Chihuahua 31136, Mexico

charge and discharge processes. ZAB has been widely used because it exhibits high energy density, high availability and low pollution compared to lead acid batteries, redox flow cell, sodium/sulphur batteries, and lithium-ion batteries. That is why ZAB is currently one of the most promising candidates for energy storage [10, 11]. Although ZAB has a lower theoretical specific energy than Li-air batteries (~1350 Wh kg^{-1}), they are four times higher than Li-ion batteries [9]. Finally, ZAB uses aqueous electrolytes, because of its low cost which and higher conductivity values [7].

Hydrogels are quite hydrophilic polymer networks, either synthetic or natural, usually stabilized by covalent bonds or non-covalent interactions between the chain of macromolecules, known as cross-linking. Several biopolymers such as starch, chitosan, collagen, and cellulose have been described as suitable biomaterials for the development of hydrogels (GPEs) with potential application for energy storage. Especially starch (A) and its derivatives have attracted the interest of many scientists for the development of industrial applications because of their cost-effectiveness, renewable nature, abundance in nature, and biodegradability [12]. However, their limitations include poor stability and mechanical properties, high hydrophilicity, and fragility. These drawbacks need to be reduced to enhance the quality of these materials. Chitosan (CS) is a cationic biodegradable biopolymer obtained from chitin of crustaceans after deacetylation with an alkaline treatment [13]. The presence of hydroxyl and amino groups in its molecular structure provide higher hydrophilicity in the cells, resulting in benefits to the GPEs operation. Due to its biocompatibility, biodegradability, nontoxicity, and absorption behavior, chitosan is a valuable suitable functional material for polymer electrolyte applications [14]. Moreover, chitosan can preserve its chemical and thermal stability until ~200 °C with adequate mechanical strength [15]. Based on the advantages of starch and chitosan, it is expected that a blend of both polymers would be able to form a biodegradable film with better mechanical properties and lower water permeability [16]. Various reagents such as glutaraldehyde, boric acid, epichlorohydrin, and glyoxal, have been implemented to modify these biomaterials by chemical crosslinking [17]. Specifically, epichlorohydrin (ECH) has been employed as a crosslinker which leads to the formation of glycidylether linkage within CS and A to improve the thermal and structural properties of the hydrogels.

KOH solution has been used as an ion source to enhance the ionic conductivity of the electrolyte. Iles et al. [7] reported an ionic conductivity of 0.019 $S{\cdot}cm^{-1}$ using a GPE synthetized applying the solution casting technique based on vinyl acetate, butyl acrylate, and vinyl neodecanoate in form of a terpolymer (VAVTD), polyvinyl alcohol (PVA) and KOH 12 M solution [7].

The present study reports the synthesis of GPEs based on chitosan and avocado starch crosslinked with ECH using a solution casting method. The effect of different ratios of avocado seed starch on the functional properties of the hydrogels have been studied in dried form and when swelled in 12 M KOH solution. Attenuated Total Reflectance Fourier Transform Infrared Spectroscopy, X-Ray Diffraction, and Thermogravimetric Analysis were used to study the effect of ECH on the crosslinking of the biopolymers. In addition, by means of Potential Electrochemical Impedance Spectroscopy and Cyclic Voltammetry the electrochemical properties of the synthesized membranes were evaluated. The obtained results with these techniques indicated that the synthesized material is a promising material for application as hydrogel electrolyte in ZABs., as it presents the promising properties of the biopolymer materials in energy applications, as synergy with other components, tunable properties, safety, biocompability and renewability.

Experimental

Materials and methods

In this work, food grade chitosan (90.6% deacetylated [18]) was used (Purity: 100%, BioFitnest). Starch was synthesized from avocado seeds in the laboratories of Yachay Tech University according to the protocol previously reported [19]. Anhydrous glacial acetic acid (Density: 1.05 kg/L, Purity: 100%), ECH of analytical grade and anhydrous KOH pellets (purity ≥ 85.00%) were purchased from Sigma Aldrich. The solvent used in all solutions was distilled water. The Pt plates (99.97%) and Zn discs (99.999%) utilized in the testing were acquired from Goodfellow.

Preparation of the CS and CS: a hydrogels

Hydrogels were synthesized using the solution casting method in a two-step synthesis procedure; 3.5 g of CS was dissolved in 100 mL of 1% (v/v) acetic acid solution and 3.5 g of avocado starch in 100 mL of distilled water at 80 °C. The polymer solutions were stirred for 3 h until homogenous solutions were obtained. After that, 5% wt. of ECH in different volume of polymers' ratio were added to the hydrogels' solution, varying the amount of avocado starch (Table 1) under continuous stirring for 1 h. Then, the mixtures were placed in Petri dishes and allowed to dry at room temperature for one week. A GPE without starch was prepared to contrast the results generated by the crosslinker. Finally, the resulting films were stored in a desiccator for further characterization in dry form. Additionally, another set of GPEs were immersed in a 12 M KOH solution during 48 h before

Table 1 Codes to designate the gel polymer electrolytes

Electrolyte	Hydrogel Code
Chitosan	CS
Chitosan:Avocado Starch (3:1)	CS:A 3:1
Chitosan:Avocado Starch (3:2)	CS:A 3:2
Chitosan:Avocado Starch (3:3)	CS:A 3:3
Chitosan KOH 12 M	CS Sw
Chitosan:Avocado Starch (3:1) KOH 12 M	CS:A 3:1 Sw
Chitosan:Avocado Starch (3:2) KOH 12 M	CS:A 3:2 Sw
Chitosan:Avocado Starch (3:3) KOH 12 M	CS:A 3:3 Sw

further characterization techniques. To label the soaked membranes "Sw" was added to the GPE codes (Table 1).

Swelling behavior of the hydrogels

For swelling ratio (SR) calculations, the samples were weighed before and after 48 h of being immersed in 12 M KOH solution. After that, the SR was determined using Eq. (1):

$$SR = \frac{W_T - W_0}{W_0}\ x\ 100\% \tag{1}$$

where W is volume or weight, and the subindexes $_T$ and $_0$ are the swollen GPE and the initial GPE, respectively.

Structural, thermal, and electrochemical characterization

ATR-FTIR methods

Functional groups of the CS and A biopolymers and the synthetized hydrogels were analyzed by FT-Infrared Spectroscopy (FTIR), that was conducted in the solid-state by total attenuated reflectance (ATR) using a Cary 630 (Agilent Technologies Inc. Santa Clara, CA, USA) equipped with 1-Bounce Diamond ATR accessory. Spectra were acquired in the $4000-400\ cm^{-1}$ range, with a resolution of $4\ cm^{-1}$ and 64 scans.

X-Ray diffraction

The X-ray diffraction (XRD) technique was used to determine the crystallinity and amorphousness of the GPEs at room temperature. X-ray diffractograms were obtained with a computer-controlled Rigaku Mini-flex-600, with a D/tex Ultra 2 detector 26 (Rigaku, Tokyo, Japan), and the X-Ray generator in a sealed tube with a Ni-filtered Cu Kα radiation source (λ = 0.15418 nm, 40 kV, 15 mA). For data collection, samples were placed on a sample holder; and the selected angular region was $2\theta = 5° - 80°$ with a step width of 0.01°. The degree of crystallinity X_c was calculated using Match! Software [20].

Thermal analysis

The thermal properties of the membranes were analyzed by thermogravimetric analysis (TGA) in the range of 25 to 800 °C with a heating rate of 10 °C/min, using a Q600 DSC-TGA (TA Instruments, New Castle, DE, USA) under nitrogen atmosphere on samples of 5–10 mg.

SEM and BET characterization

To analyze the hydrogel's morphology, scanning electron microscopy was used (SEM, JEOL JSM-6010/LV microscope, JEOL Ltd., Japan N_2 adsorption/desorption isotherms at −195 °C were performed with a Quantachrome® S–BET Autosorb iQ2 (Quantachrome Instruments, USA) to develop). Brunauer–Emmett–Teller (BET). Each membrane was heated at 80 °C in a vacuum for 1 h before the adsorption/desorption test. Elemental analysis by EDS (Energy Dispersive Spectroscopy) was performed on the swelled membranes with the mentioned SEM equipment.

Electrochemical measurements

Electrochemical impedance spectroscopy (EIS) studies were performed using a VIONIC instrument, (Metrohm model, Ecuador), to evaluate the electrochemical behavior of the hydrogels. The EIS frequency range worked was from 100 kHz to 1 Hz, with two Pt plates holding the electrolyte in the cell configuration, with a 1 cm^2 area of Pt electrodes acting as blocking electrodes. The conductivity and temperature relationship were examined using a Julabo (−40 °C, 15 L) Ref. Circulator from Polyscience, in the range of 0 to 50 °C with ± 1 °C precision, after 5 min of stabilization. The ionic conductivity, σ, was calculated using Eq. (2):

$$\sigma = \frac{l}{A * R_b} \tag{2}$$

where A is the Pt plate area, l is the GPE thickness, and R_b is the bulk resistance, prevenient from the intersections of the Nyquist curve with the x-axis. Quadrupled impedance measurements were carried out for each GPE. The activation energy (Ea) of each electrolyte was determined by, the Arrhenius Eq. (3) with a linear fitting by plotting the relationship between ln(σ) and 1000/T:

$$\sigma = \sigma_0 \exp[-\frac{Ea}{K_b(T)}] \tag{3}$$

where K_b is the Boltzmann's constant, σ_0 is a pre-exponential factor, and T is the absolute temperature. Linear Sweep Voltammetry (LSV) staircase of hydrogels was registered between 0.0 V and +3.0 V at a speed of 1 mV•s^{-1} using a Zn/Hydrogel/Pt cell where Zn disc was used as the counter and reference electrode, and Pt served as the working electrode. CV study was carried out using a Zn/hydrogel/Zn symmetric cell with Zn electrodes of 1 cm^2 and a scanning speed of 100 mV/s in a symmetric potential window from −1.5 V to +1.5 V. OriginPro software was used for data processing.

Battery tests

Battery tests were performed in a potentiostat/galvanostat AMETEK® VersaSTAT 3 model (Princeton Applied Research, Berwyn, IL, USA), with a sandwich model consisting of the GPE between the anode and cathode. The anode was made of a piece of polished high-purity Zn foil (15 × 10 mm length and width and 0.2 mm in depth, purity 99.9%, Yunexpress Inc., China). The cathode used was Pt/C (20% wt.), SIGRACET® B slides (15 × 10 mm length and width, and 0.4 mm in depth) impregnated with 1 mg/cm^2 commercial catalytic ink were used as cathode. The discharge current density was −3 mA/cm^2 and the cut-off voltage was 0.2 V. The specific capacitance was determined by weighing the zinc loss after discharging the Zn-air battery at 1.98 mA/cm^2.

Results and discussion

Reaction mechanism of the hydrogels

Reaction of biopolymers with ECH is reported on basic medium (pH 10.0) [17, 21]. Herein crosslinking with epichlorohydrin in an acidic condition was studied because of the presence of acetic acid from chitosan solution, already reported by Chen et al. [22]. Epichlorohydrin acts as the crosslinker in the reaction by leading to the formation of the glycidylether linkage (Fig. 1b) through the reactions with hydroxyl groups of the glycan structure [23]. With this reaction it is expected to enhance the thermal and structural properties by the reinforcement of the intermolecular binding with the introduction of covalent bonds to supplant natural hydrogen bonds (Fig. 1a) formed when the amino group from chitosan and the hydroxyl group from starch interact [24]. Some chemical structures formed by the proposed reaction can be ascribed (Fig. 1c). The desired product of the reaction with ECH is depicted in Fig. 1c (III). The structures resulting from the cross-linking reaction between the hydroxyl groups of chitosan and adjacent starches are depicted in (II) and (IV), respectively. The terminal tails (I) and (V) can be formed by the reaction of excess water with ECH; and (VI) is the reaction product between the two biopolymers without ECH.

Structural characterization

ATR-FTIR analysis

For the avocado seed starch, it was identified the characteristic bands at 3310 cm^{-1}, 2925 cm^{-1}, and 1024 cm^{-1}, corresponding to the O–H, and C–H stretches and to the pyranose ring respectively C–O–C (Fig. 2a, b). The bands at 1636 cm^{-1} and 1423 cm^{-1} were assigned to the O–H and –CH_2 bending. The molecular structures of starch and chitosan are alike, except that the amino group existing only in chitosan at C-2 position as same as its counterpart –OH in starch (Fig. 1). The IR spectra for CS presented a band at 2925 cm^{-1}, attributed to C–H stretching vibration [25]. The broad band at 3400 cm^{-1} was related to the hydroxyl groups, reported to contribute to the complex vibrational stretches associated with the free intramolecular bound hydroxyl groups [26]. Other band was presented at around 1636 cm^{-1}, corresponding to the O—H bending of water. This band usually overlaps with the C=O band corresponding to the carboxamide of the remained acetylated group (amide I) of chitosan, as reported by Liu et al. [27]. The band at 1546 cm^{-1} was identified for the primary amine N–H bending vibration, comparable to the values reported by Kadir et al. [28]. The band at 1024 cm^{-1} in the fingerprint region for both chitosan and starch was attributed to the signals of glycosidic bonds [29]. The IR spectra for the synthetized hydrogels with ECH presented the same mentioned bands but with intensity variations. These changes evidenced some physical or chemical interactions between the mixed substances [17, 30], as proposed in Fig. 1.

For the swelled membranes in KOH 12 M (Fig. 2c), relevant changes were observed in the O−H and C−H regions, with a notorious increase of the band at 3280 cm^{-1} caused by the water insertion, with a higher amount of hydrogen bonds within the polymeric matrix [7]. The already mentioned peak at 2925 cm^{-1} attributed to the C−H stretching vibration shifts to a lower wavenumber at 2910 cm^{-1} when immersed in KOH. For the amine band, it significantly reduced its intensity and shifted to a higher frequency of 1574 cm^{-1}. This could be attributed to a more amorphous state because of the presence of more hydroxyl groups [31]. The band corresponding to the O—H bending of water shifted to 1646 cm^{-1}. The band representing the ring's C−O−C skeletal vibration also shifted to a lower wavenumber (1014 cm^{-1}), suggesting the interaction of K^+ with the polymeric chain [32].

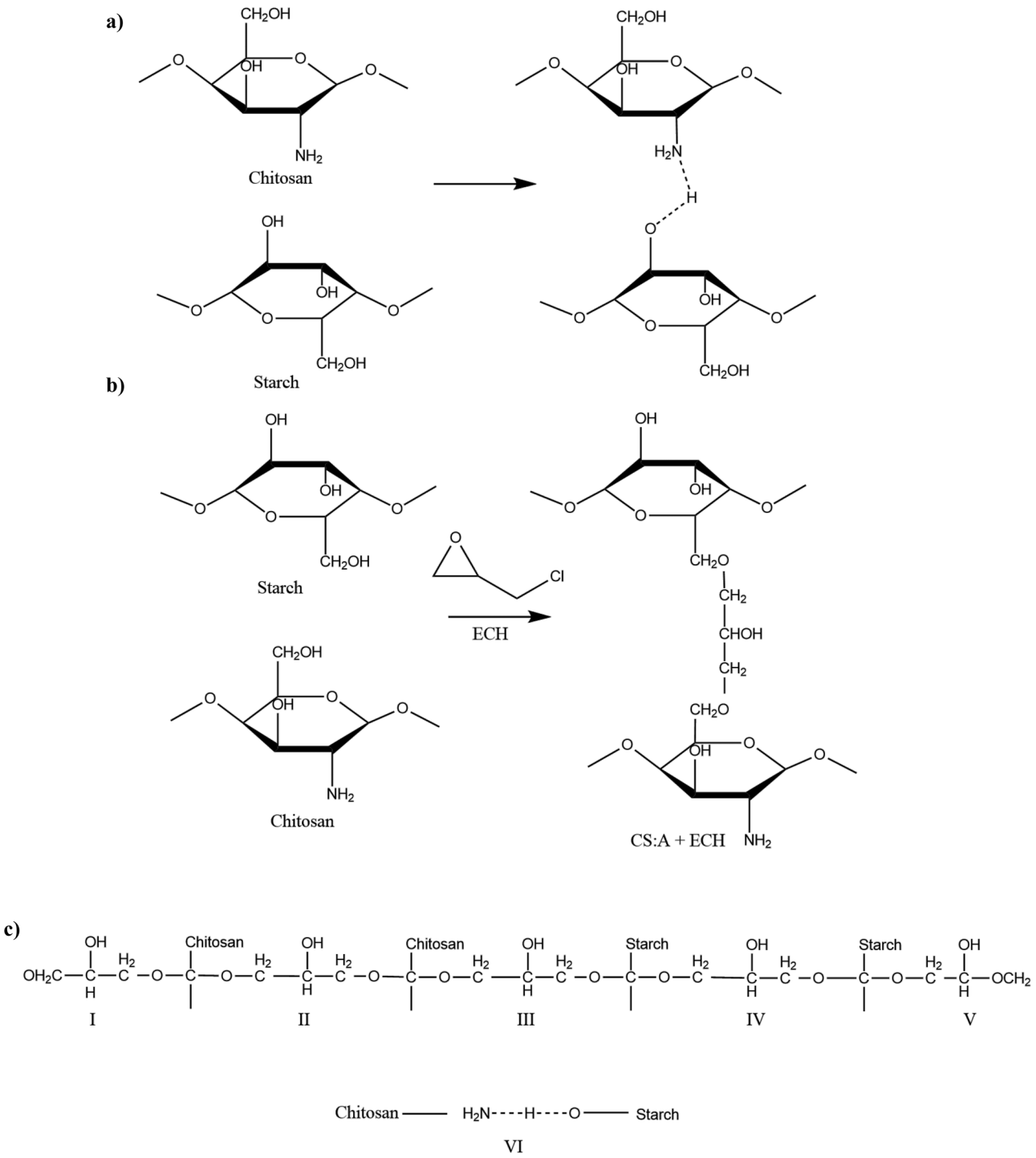

Fig. 1 Schematic representation for the proposed reaction mechanism of hydrogels composed of **a** CS-A without ECH **b** CS-A with ECH, **c** structures formed by the crosslinking reaction of ECH

XRD Analysis

The predominant broad peak in each film without immersion in the alkaline solution was identified at approximately $2\theta = 21°$ pointing to a high amorphousness of the synthesized GPEs (Fig. 3). The chitosan diffractogram evidenced its semicrystalline structure, mainly maintained by intramolecular and intermolecular interactions [33]. Its rigid structure is due to the hydrogen bonds formed among amino and hydroxyl with a water molecule inside the network [2].

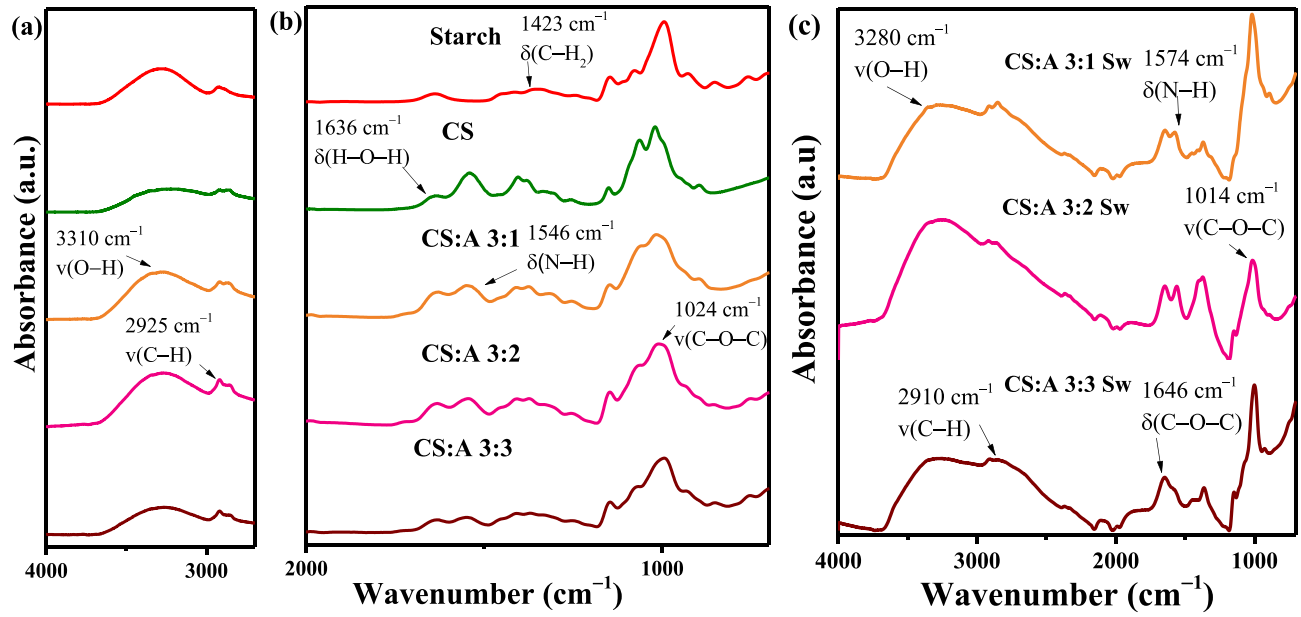

Fig. 2 ATR-FTIR spectra of CS, CS:A membranes **a**-**b** before and **c** after immersion in 12 M KOH solution

The peak at 2θ = 19° is characteristic of the crystalline behavior of pure chitosan and starch [34]. In addition, the membranes showed different intensities before and after immersion in 12 M KOH solution (Fig. 3). The broad and large peaks are related to the amorphous region, while the narrow and sharp peaks represent the crystalline part of the films. Swelling membranes presented a considerable intensity decrease because of the addition of the 12 M KOH solution; this result was expected as it is associated with the reduction of crystallinity [35]. Additionally, the broad peaks indicated the increase of the amorphous domain and the upgrowth of the molecular mobility of the ions [36, 37].

The degree of crystallinity of the membranes is relevant since it is related to the swelling behavior of hydrogels [38]. For the gels immersed in 12 M KOH, the reduction of X_c was observed (Table 2). The CS:A 3:1 Sw showed the lowest X_c value (11.96%) while the values for CS:A 3:2 Sw and CS:A 3:3 Sw were 13.42% and 13.08%, respectively. Consequently, CS:A 3:1 Sw film contained a highly amorphous region and therefore it was expected to conduct ionically better. Crystallinity is associated with the swelling behavior of hydrogels, and ionic conductivity increases with decreasing crystallinity because ions have low mobility in the crystalline phase [38]. In addition, a larger amorphous region has more voids present which are related to higher ionic conductivity values [39]. The complex formed between the polysaccharide chains and the K^+ could be attributed to this behavior and thus the crystallinity decrease could be related to the hydrogen bonding destruction in the matrix [40].

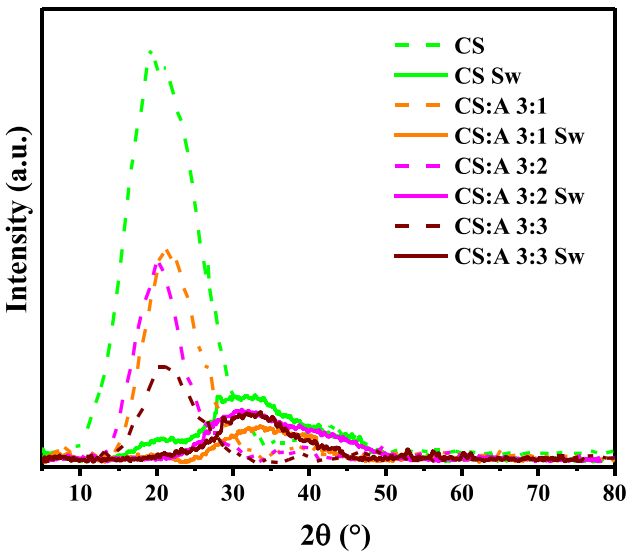

Fig. 3 XRD patterns of CS and CS:A at different proportions of starch before and after being immersed in 12 M KOH solution

Table 2 Crystallinity degree for the GPEs calculated from the XRD pattern

Electrolyte	X_c (%)
CS	22.22
CS:A 3:1	17.32
CS:A 3:2	15.84
CS:A 3:3	15.13
CS Sw	12.90
CS:A 3:1 Sw	11.96
CS:A 3:2 Sw	13.42
CS:A 3:3 Sw	13.08

SEM and BET analysis

The N_2 adsorption-desorption isotherms for the membranes were investigated (Fig. S1). A low surface area of 2.67 m^2/g is obtained for the CS:A 3:3 membrane (representative data for the proposed membranes), along with the hysteresis loop pointing to a mixture of type II and III isotherms. This result suggests that the membranes are non-porous or macroporous materials, characterized by a low adsorbent-to-adsorbate ratio, thus performing absorption rather than adsorption processes. SEM micrographs obtained for the dried CS:A 3:3 membrane (Fig. 4a, b) suggested the complete interaction of starch and chitosan since no starch granules were observed on the surface, similar to the results reported by Yusof et al. [41]. Moreover, the chapped surface might indicate the formation of a porous structure in which the ionic salt could enter the matrix. The obtention of a porous structure is relevant due to its essential role in transporting the charge carriers in the system [42]. Once the membrane had absorbed the ionic salt solution, granules were observed on the GPE's surface (Fig. 3c). EDS elemental mapping was performed on the swollen membranes (Fig. 4d), evidencing the dispersion of the added KOH within the polymer electrolyte all over the surface, confirming the complexation of the salt withing the polymer matrix. The presence of free Cl^- ions in zone 002 originated from unreacted ECH traces that reacted with K^+ ions could be causing the agglomeration of deposited KCl salt over the membrane [43]. On the other hand, in zone 001 the decrease in intensity of C and O mass percentage could suggest the good blending nature with the added salt [44].

Thermal analysis

The dry membrane showed three degradation regions at 200, 300, and ~450 °C (Fig. 5a). The total weight losses in the first region at ~200 °C of CS:A 3:1, CS:A 2:2, CS:A 3:3 were 10.44%, 6.05%, and 9.24% by weight, respectively. This first weight loss region is related to

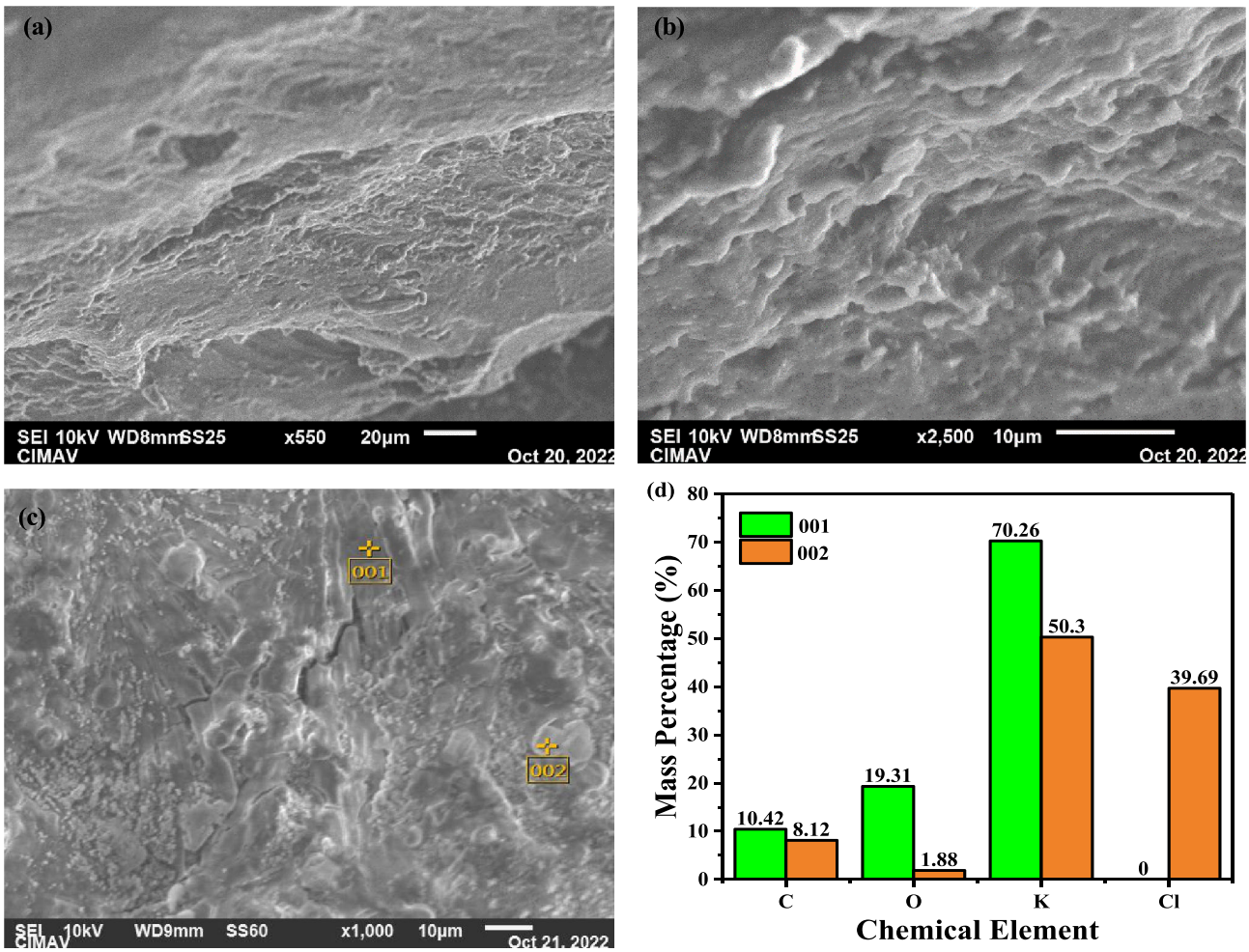

Fig. 4 SEM micrographs of the CS:A 3:3 membrane at **a** 550× and **b** 2500× and the CS:A 3:3 Sw membrane **c** at 1000x **d** elemental composition of the CS:A 3:3 Sw polymer electrolyte performed at **c** 001 and 002

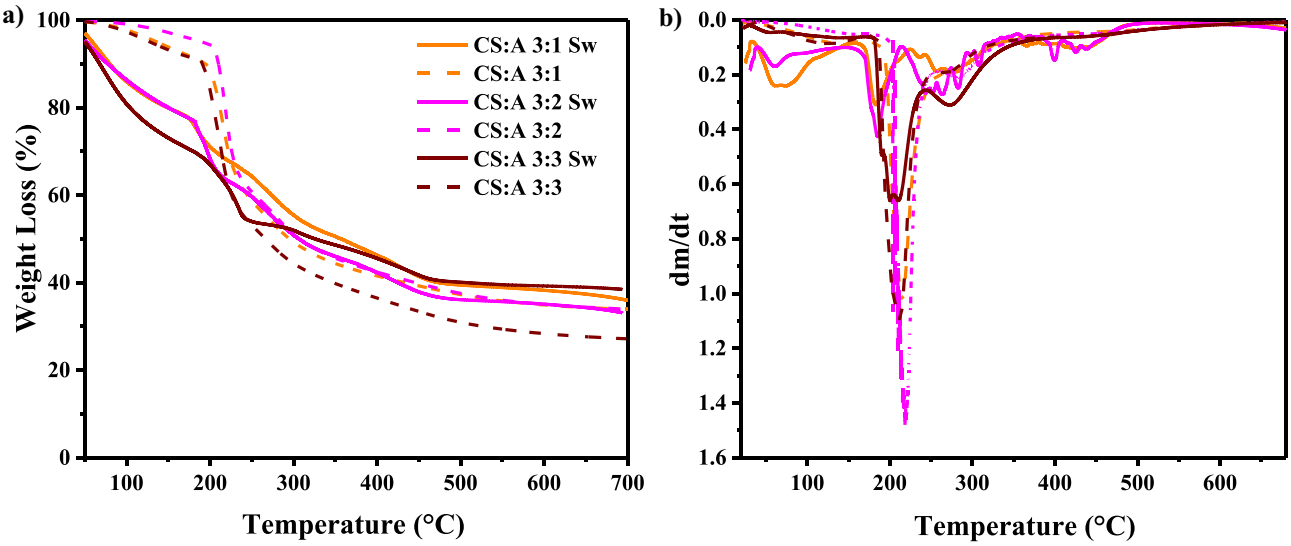

Fig. 5 **a** Thermal stability studies of the CS:A and CS:A Sw at different starch proportions. **b** DTGA curves of electrolytes

the of internal water loss in the matrixes [45]. The second loss beyond 300 °C is related to the char formation of chitosan [45, 46]. Furthermore, above ~450 °C, the remaining weight was relatively constant, with a residual of 39.23 wt%, 39.74 wt% and 33.38 wt% for CS:A 3:1, CS:A 3:2 ,and CS:A 3:3, respectively. This slight variation indicates a higher carbon yield with the matrixes incorporating starch. Therefore, the TGA curves evidenced that the thermal resistance increased when starch polymer and epichlorohydrin were added, indicating that thermal degradation of the chitosan-starch GPEs is reduced after the film modification [7].

Regarding the swollen membranes, the first range was observed between 55 and 150 °C with a weight loss of 22.47%, 22.80%, 29.62% for CS:A 3:1, CS:A 3:2, CS:A 3:3, respectively and is related to the evaporation of water present in the polymeric chains upon immersion in the 12 M KOH solution [18]. Next, the second range was observed between 150 and 250 °C, and it is possible to attribute it to the degradation of the saccharide backbone, suggesting the dehydration of the saccharide rings takes place [47]. From the derivate TGA (DTGA) curves (Fig. 5b), it was observed that the modification of the chemical structure led to a decrease in bond strength, pointing to some degree of weakening of the interactions of the synthesized membranes compared to the pure CS films. It was also evidenced that a higher percentage of residues in the swollen GPEs in contrast to the dried membranes could point to the presence of potassium oxide salts formed upon KOH decomposition [48].

Electrochemical characterization

Swelling ratio and conductivity

The synthesized electrolytes were immersed in 12 M KOH solution to allow the water molecules to enter the polymeric system and thus enhance the electrochemical properties. The swelling ratio (SR) was calculated according to Eq. (1) to measure the percentage of KOH absorption (Table 3). It is observed that the non-crosslinked chitosan membrane achieved the highest KOH uptake with a SR value of 126.2%. Nonetheless, its electrochemical properties, such as the reversibility of cyclic voltammetry studies, was greatly affected; so, it was necessary to add starch to improve its resistance. In the case of the crosslinked hydrogels, it is observed that increasing the proportion of starch also improved the membrane's absorption from 77.4 to 94.5% (Fig. 6; Table 3). It is also evident that an increase in the SR increases the ionic conductivity of electrolytes. The maximum ionic conductivity of the polymeric membranes achieved was 0.027 $S \cdot cm^{-1}$ for the CS:A 3:3 Sw membrane at 30 °C. The alkaline solution is the ionic species donor in the electrolyte that increase the ionic conductivity of the synthetized membranes when it penetrates the polymer skeleton [49].

Activation energy

The plots of ln (σ) versus 1000/T for each curve conformed to a linear behavior, suggesting a dependence between the ionic

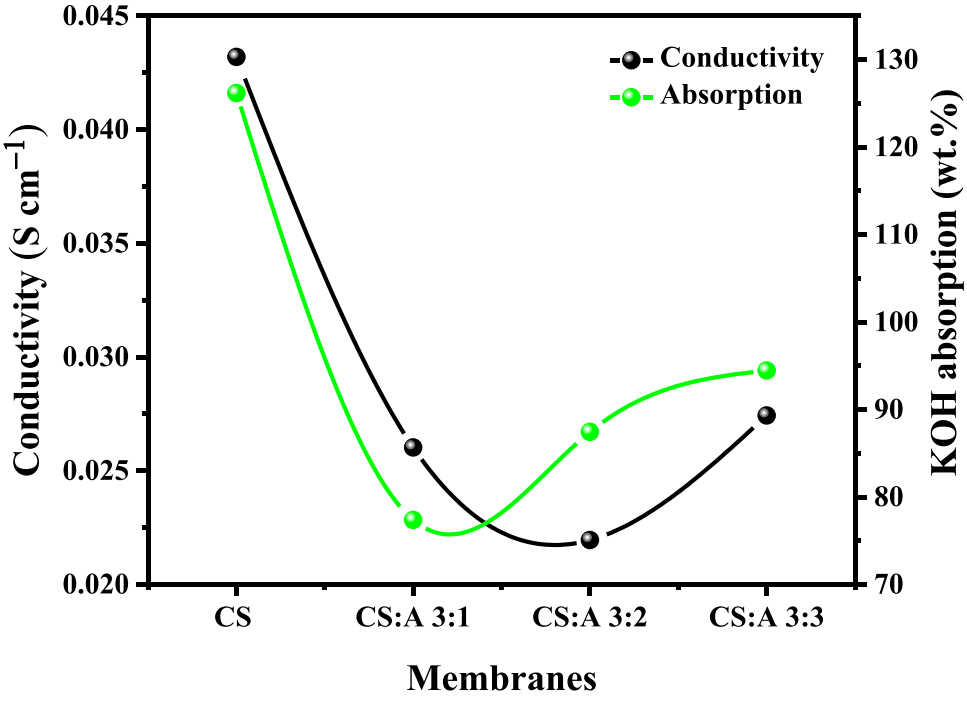

Fig. 6 Comparison within the ionic conductivity values at 30 °C and 12 M KOH solution absorption of the hydrogels

conductivity (σ) and the temperature (Fig. 7). It can be inferred that the results satisfy the Arrhenius behavior, related to the conductivity as a thermally assisted process [50]. For the conduction process to take place the energy barrier must be overcome so that the movement of the ions from one site to another occur [51]. The activation energy (E_a) was determined as the slope of each curve. The CS:A 3:2 Sw hydrogel achieved the highest value of E_a, with 0.373 eV. Lower values of 0.244 and 0.295 eV were obtained for the CS:A 3:1 Sw and CS:A 3:3 Sw, respectively.

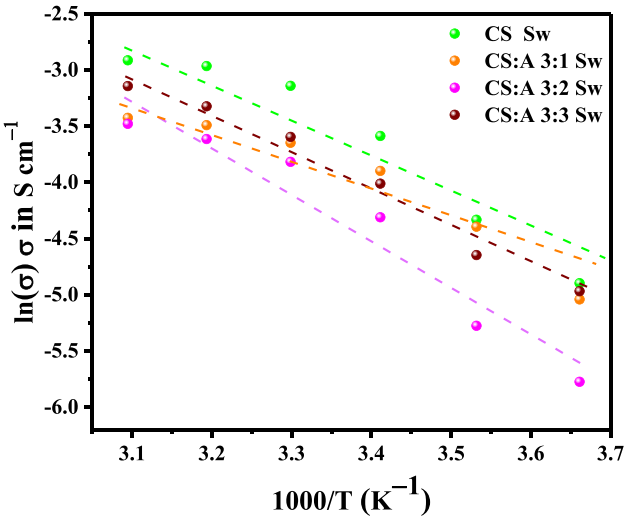

Fig. 7 Temperature dependence of ionic conductivity of chitosan-starch electrolytes

When the starch content was increased, the absorption capability increased (Table 3), hence a higher conductivity was evidenced. The ionic conductivity values rise due to the higher ionic concentration inside the GPEs, which is attributed to the great amorphousness and the higher separation of the chains, as demonstrated by the XRD results. In addition, the hydrogels showed activation energy values which decrease when the starch content increases, meaning that the highest the amount of KOH that penetrates the GPEs, the highest the conductivity and hence, the lowest the required energy that must be provided to ionic conduction. CS film presented higher E_a values suggesting that pure chitosan restricts ion mobility resulting in lower ionic conductivity. However, this membrane does not meet the trend mentioned above since it absorbs the largest amount of KOH solution but accomplishes a lower conductivity value; this could be explained by the low structural integrity of the hydrogel.

Table 3 Swelling ratio (SR), activation energy (Ea), and conductivity (σ) value for each electrolyte after incubation in 12 M KOH solution. σ values were obtained at T = 30 °C

Electrolyte	SR (%)	Ea (eV)	σ(S/cm)
CS	126.2	0.319	0.043
CS:A 3:1 Sw	77.4	0.244	0.026
CS:A 3:2 Sw	87.5	0.373	0.022
CS:A 3:3 Sw	94.5	0.295	0.027

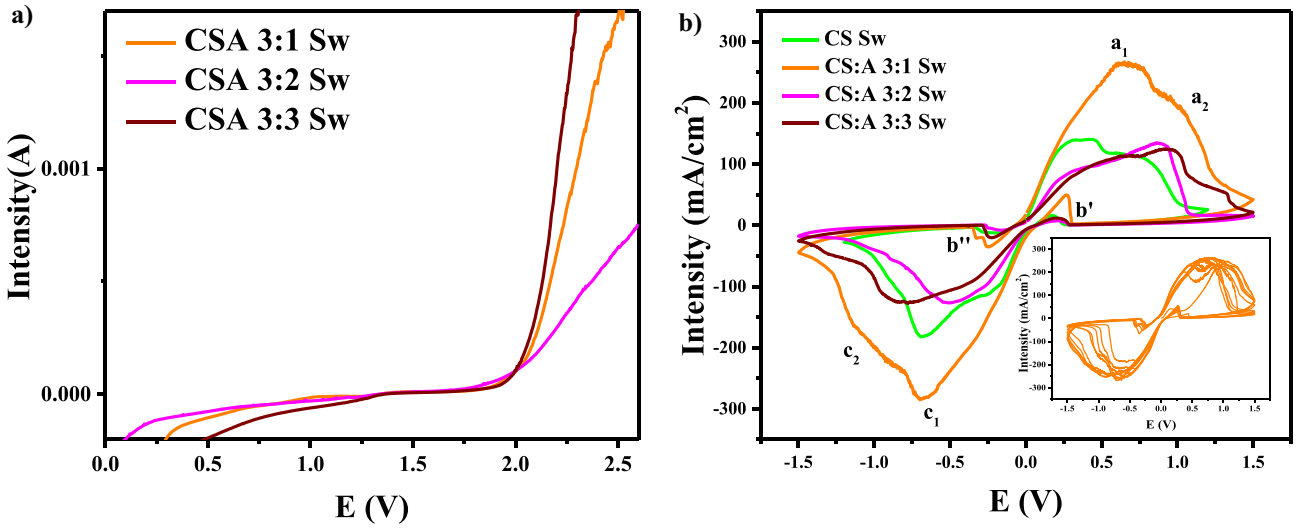

Fig. 8 **a** Linear sweep voltammetry studies for the CS:A Sw GPEs at different starch proportions. **b** Cyclic voltammograms (100 mV/s scan rate and potential range from −1.5 V to + 1.5 V) of Zn/GPEs/Zn symmetric cells for pure CS, CS + ECH, CS:A 3:1, 3:2 and 3:3 @in 12 M KOH solution. Inset: 30 consecutive cycles of CS:A 3:1 membrane in 12 M KOH solution

Linear Sweep and cyclic voltammetry

The electrochemical stability of the chitosan-starch membranes has a significant impact in the long-term efficiency of the zinc-air batteries. The electrochemical window is considered a fundamental parameter to evaluate the electrochemical stability of the GPEs. The current flow remained stable when the voltage is below 1.8 V (Fig. 8a). Beyond this point, the current increased immediately, indicating that the GPE was rapidly decomposing. In addition, the electrochemical window of the GPEs is almost ~1.8 V compared with some liquid electrolytes with an electrochemical window of 1.23 V, which is restricted due to water electrolysis. From cyclic voltammetry studies, the membranes underwent oxidation and reduction, as observed through the redox peaks (Fig. 8b). The anodic peaks a_1 and a_2 were ascribed to the oxidation of Zn to $Zn(OH)_4^{2-}$ and Zn to $Zn(OH)_3^-$ respectively [52]. The last compound is formed because of the OH^- depletion in the proximity of the electrode surface, resulting in a prepassive layer at a more positive potential than the peak a_1. The cathodic peaks c_1 and c_2 were attributed to the reduction of Zn^{2+} to Zn. The peaks b' and b'' represented the oxidation of Zn after the dissolution of the passive film deposited on the electrode surface, which comes off during the cathodic and anodic scan, respectively [52].

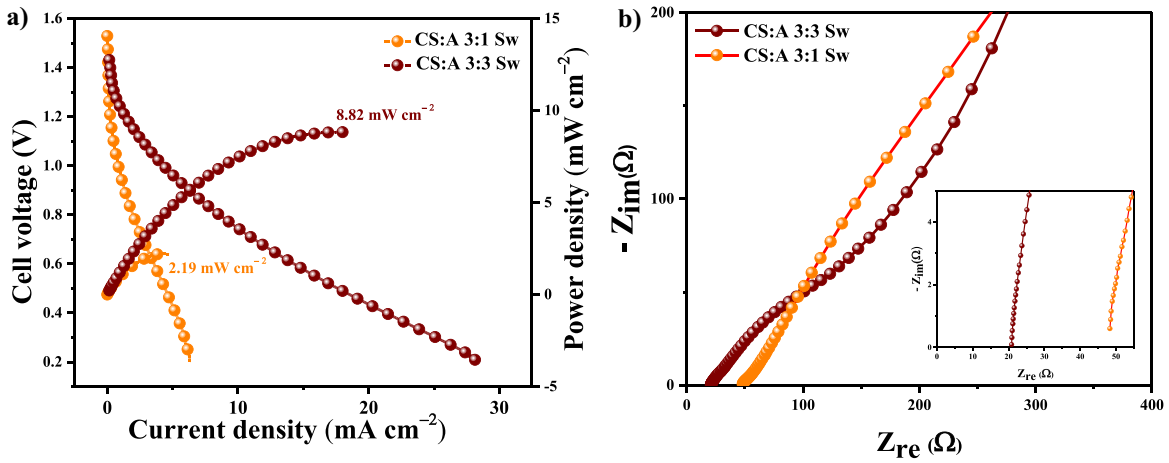

Fig. 9 **a** Polarization curves for the battery operated with the synthesized GPEs; **b** potential electrochemical impedance spectroscopy studies

Table 4 Battery performance in batteries with similar polymer electrolytes

Electrolyte	Ionic Conductivity $\times 10^{-3}$ ($S \cdot cm^{-1}$)	Bulk Resistance (Ω)	Current Density ($mA \cdot cm^{-2}$)	Power Density ($mW \cdot cm^{-2}$)	Reference
CS:EC:NH_4NO_3	9.93	29.8	16.0	8.70	[55]
Cornstarch:PVP: $NH_4CH_3CO_2$	1.09×10^{-3}	-	0.07	0.06	[56]
Cornstarch:CS: NH_4I	1.28	62.30	17.70	4.00	[42]
LC:Starch: $LiPF_6$	1.27	~25	~16	-	[57]
CS:Starch:NH_4SCN	0.13	-	-	-	[58]
CS:A:ECH:KOH	30	20.85	28.27	8.82	This work

CS:A 3:1 Sw was the hydrogel with the best electrochemical behavior with an intensity superior to 260 $mA \cdot cm^{-2}$. The Figure inset represented the stability of this membrane with 30 consecutive cycles registered; this behavior confirmed the reversibility and stability of this system. All membranes presented a quasi-reversible redox behavior ensuring the ionic transport of the GPEs. In addition, an improvement in the intensity was evident due to the number of electrons transferred within the redox species and the electrode which were determined by the ions motion [52]. While chitosan is the polymer that confers the electrochemical properties to the films, starch provides mechanical properties such as resistance. The results suggest been a suitable application in energy storage devices.

Battery tests

Battery tests were performed following a cell configuration Zn/GPE/air in which Zn operates as the anode and the Pt/C as the cathode, with a configuration already reported by our investigation group [18]. The open circuit potential for the tested GPEs achieved values of 1.45 V. Discharge power density curves (Fig. 9a) exhibited a linear voltage drop with an increase of the discharge current density, suggesting that the ohmic losses dominated the cell parameter [53]. The polarization curves showed notorious differences when more starch was added to the polymer matrix, obtaining four times the current density of the battery containing the CS:A 3:1 Sw membrane (6.3 mA/cm^2) compared to the CS:A 3:3 Sw (28.3 mA/cm^2). The maximum power density of the battery assembled with the CS:A 3:3 Sw membrane was 8.83 mW/cm^2 at room temperature; this result indicates a better performance than other primary batteries of previous reports (Table 4). The bulk resistance of the batteries was studied, obtaining a minimum value of 20.85 Ω for the CS:A 3:3 sw GPE (Fig. 9b), as evidence of the existence of more charge carriers and OH^- ions that facilitate the conduction process [54]. This result is in accordance with the previously discussed characterization studies, which confirmed a higher amount of KOH solution uptake in the electrolyte, along with the amount of starch incorporated into the matrix.

Conclusions

GPEs based of CS and A were synthetized using ECH as a crosslinker reagent. ATR-FTIR spectroscopy confirmed the crosslinking reaction for CS:A:ECH of the hydrogels achieved by the proposed synthesis. In general, XRD patterns showed a broadening of the peaks with starch concentration, indicating a reduction in the degree of crystallinity due to the crosslinking reaction which leads to a good swelling degree and high-water absorption. From the swelling behavior results, the CS GPE obtained a higher SR percentage of compared to the CS:A hydrogels. However, this is affected negatively with its low structural integrity when applied in energy devices, with the addition of another polymer obtaining a superior structural stability. It was evidenced that an increase in the starch proportion in the CS:A films enhanced the membrane's absorption, and therefore ionic conduction values increased, requiring lower activation energies. Thermal analysis suggested an increase of the thermal stability when starch polymer and epichlorohydrin are added to the swollen membranes. The study of N_2 adsorption/desorption processes supported the absorption and non-adsorption mechanism. By the SEM micrographs, it was confirmed the obtention of a porous structure, essential for transporting the charge carriers in the electrolyte. EDS elemental mapping evidenced the dispersion of the added KOH. Moreover, analysis of the ionic conductivity with temperature confirmed that the GPEs presented an Arrhenius-type behavior in the range of 0 to 50 °C and a greatest conductivity of 0.027 $S \cdot cm^{-1}$ at 30 °C. The cyclic voltammetry test revealed a quasi-reversible behavior of the GPEs that was depicted during the oxidation and reduction processes, with a maximum intensity peak of ~260 $mA \cdot cm^{-2}$. The chitosan-starch GPEs were tested in a zinc-air battery prototype reaching a maximum power density of 8.82 $mW \cdot cm^2$, reaching appropriate values for the applicability of CS:A hydrogels in zinc-air batteries.

Supplementary Information The online version contains supplementary material available at https://doi.org/10.1007/s10965-023-03566-0.

Acknowledgements The authors express their gratitude to the Mexican Council of Science and Technology for supporting this work through the project Ciencia de Frontera grant # 39569 and to the Centro de Investigación en Materiales Avanzados S.C "CIMAV", for the financial support granted for the development of this research through project PI-22-05 and grant PI-23-10. Also, the authors are grateful for the technical support to Anabel de la Cruz from CIMAV. The authors acknowledge the Grupo de Investigación Aplicada en Materiales y Procesos (GIAMP), Yachay Tech University for their collaboration through some of the indispensable equipment for this research project.

Author contributions Formal analysis, methodology, conceptualization, investigation, writing-original draft preparation, and data curation, M.I.C.-B, M.F.B.-C.; write—review, editing, conceptualization, methodology, and supervision, V.M.C., J.B., L.Á.-C., and J.P.T.; project administration, L.Á.-C. and J.P.T.; funding acquisition, L.Á.-C. All authors have read and agreed to the published version of the manuscript.

Data availability The data that support the findings of this study are available from the corresponding author, Juan P. Tafur, upon reasonable request.

Declarations

Conflict of interest There are no conflicts of interest to declare.

References

1. Fenton DE, Parker JM (1973) Complexes of alkali metal ions with poly (ethylene oxide). Polym (Guildf) 14:589. https://doi.org/10.1016/0032-3861(73)90146-8
2. Armand M (1990) Polymers with ionic conductivity. Adv Mater 2:278–286. https://doi.org/10.1002/ADMA.19900020603
3. Aziz SB, Abidin ZHZ (2015) Ion-transport study in nanocomposite solid polymer electrolytes based on chitosan: electrical and dielectric analysis. J Appl Polym Sci 132:41774. https://doi.org/10.1002/app.41774
4. Li Q, Itoh T, Imanishi N et al (2003) All solid lithium polymer batteries with a novel composite polymer electrolyte. Solid State Ionics 159:97–109. https://doi.org/10.1016/S0167-2738(03)00004-3
5. Asnawi ASFM, Aziz SB, Nofal MM et al (2020) Metal complex as a novel approach to enhance the amorphous phase and improve the EDLC performance of plasticized proton conducting Chitosan-based polymer electrolyte. Membr (Basel) 10:132. https://doi.org/10.3390/membranes10060132
6. Zhou D, Shanmukaraj D, Tkacheva A et al (2019) Polymer electrolytes for lithium-based batteries: advances and prospects. Chem 5:2326–2352. https://doi.org/10.1016/j.chempr.2019.05.009
7. Iles Velez AA, Reyes E, Diaz-Barrios A et al (2021) Properties of the PVA-VAVTD KOH blend as a gel polymer electrolyte for zinc batteries. Gels 7:256. https://doi.org/10.3390/gels7040256
8. Pourzolfaghar H, Hosseini S, Zuki FM et al (2021) Recent advancements to mitigate zinc oxide formation in zinc-air batteries: a technical review. Mater Today Commun 29:102954. https://doi.org/10.1016/j.mtcomm.2021.102954
9. Pan J, Xu YY, Yang H et al (2018) Advanced architectures and relatives of air electrodes in Zn–Air batteries. Adv Sci 5:1700691. https://doi.org/10.1002/advs.201700691
10. Pei P, Wang K, Ma Z (2014) Technologies for extending zinc–air battery's cyclelife: a review. Appl Energy 128:315–324. https://doi.org/10.1016/j.apenergy.2014.04.095
11. Hadjipaschalis I, Poullikkas A, Efthimiou V (2009) Overview of current and future energy storage technologies for electric power applications. Renew Sustain Energy Rev 13:1513–1522. https://doi.org/10.1016/j.rser.2008.09.028
12. Liu H, Adhikari R, Guo Q, Adhikari B (2013) Preparation and characterization of glycerol plasticized (high-amylose) starch–chitosan films. J Food Eng 116:588–597. https://doi.org/10.1016/j.jfoodeng.2012.12.037
13. Yang JK, Shih IL, Tzeng YM, Wang SL (2000) Production and purification of protease from a Bacillus subtilis that can deproteinize crustacean wastes☆. Enzyme Microb Technol 26:406–413. https://doi.org/10.1016/S0141-0229(99)00164-7
14. Rahman NA, Hanifah SA, Mobarak NN et al (2021) Chitosan as a paradigm for biopolymer electrolytes in solid-state dye-sensitised solar cells. Polym (Guildf) 230:124092. https://doi.org/10.1016/j.polymer.2021.124092
15. Krajewska B (2001) Diffusional properties of chitosan hydrogel membranes. J Chem Technol Biotechnol 76:636–642. https://doi.org/10.1002/jctb.429
16. Bangyekan C, Aht-Ong D, Srikulkit K (2006) Preparation and properties evaluation of chitosan-coated cassava starch films. Carbohydr Polym 63:61–71. https://doi.org/10.1016/j.carbpol.2005.07.032
17. Wan Ngah WS, Hanafiah MAKM, Yong SS (2008) Adsorption of humic acid from aqueous solutions on crosslinked chitosan–epichlorohydrin beads: kinetics and isotherm studies. Colloids Surf B Biointerfaces 65:18–24. https://doi.org/10.1016/J.COLSURFB.2008.02.007
18. Bósquez-Cáceres MF, De Lima L, Morera Córdova V et al (2022) Chitosan-carboxymethylcellulose hydrogels as electrolytes for zinc-air batteries: an approach to the transition towards renewable energy storage devices. Batteries 8:265. https://doi.org/10.3390/batteries8120265
19. Velasco Y, Xavier A (2022) Characterization, mechanical properties, and degradation of thermoplastic starch and cellulose blends. Universidad de Investigación de Tecnología Experimental Yachay
20. Putz H, Brandenburg K Match! - phase analysis using powder diffraction. https://www.crystalimpact.de/match. Accessed 16 Aug 2022
21. Vieira RS, Beppu MM (2006) Interaction of natural and crosslinked chitosan membranes with hg(II) ions. Colloids Surf Physicochem Eng Asp 279:196–207. https://doi.org/10.1016/j.colsurfa.2006.01.026
22. Chen AH, Liu SC, Chen CY, Chen CY (2008) Comparative adsorption of Cu(II), zn(II), and pb(II) ions in aqueous solution on the crosslinked chitosan with epichlorohydrin. J Hazard Mater 154:184–191. https://doi.org/10.1016/J.JHAZMAT.2007.10.009
23. Li W, Wei H, Liu Y et al (2021) An in situ reactive spray-drying strategy for facile preparation of starch-chitosan based hydrogel microspheres for water treatment application. Chem Eng Process - Process Intensif 168:108548. https://doi.org/10.1016/j.cep.2021.108548
24. Sreedhar B, Chattopadhyay DK, Sri M et al (2006) Thermal and Surface characterization of plasticized starch polyvinyl alcohol blends crosslinked with epichlorohydrin. J Appl Polym Sci 101:25–34. https://doi.org/10.1002/app.23145
25. El Sayed AM, El-Gamal S (2022) Synthesis, optical, and electrical properties of starch/chitosan/NaTiO3 bio-nanocomposites modified with ErCl3. Phys Scr 97:015805. https://doi.org/10.1088/1402-4896/ac40da
26. Mathew S, Brahmakumar M, Abraham TE (2006) Microstructural imaging and characterization of the mechanical, chemical, thermal, and swelling properties of starch–chitosan blend films. Biopolymers 82:176–187. https://doi.org/10.1002/bip.20480
27. Liu F, Qin B, He L, Song R (2009) Novel starch/chitosan blending membrane: antibacterial, permeable and mechanical properties.

Carbohydr Polym 78:146–150. https://doi.org/10.1016/J.CARBPOL.2009.03.021
28. Kadir MFZ, Aspanut Z, Majid SR, Arof AK (2011) FTIR studies of plasticized poly(vinyl alcohol)-chitosan blend doped with NH4NO3 polymer electrolyte membrane. Spectrochim Acta - Part A Mol Biomol Spectrosc 78:1068–1074. https://doi.org/10.1016/j.saa.2010.12.051
29. Majumdar S, Ray R (2021) Ionic conduction and charge carrier relaxation in chitosan acetate based solid biopolymer electrolyte embedded with LiClO4. J Polym Res 28:1–14. https://doi.org/10.1007/S10965-021-02509-X/METRICS
30. Chang C, Lue A, Zhang L (2008) Effects of crosslinking methods on structure and properties of cellulose/PVA hydrogels. Macromol Chem Phys 209:1266–1273. https://doi.org/10.1002/macp.200800161
31. Kasaai MR (2008) A review of several reported procedures to determine the degree of N-acetylation for chitin and chitosan using infrared spectroscopy. Carbohydr Polym 71:497–508. https://doi.org/10.1016/j.carbpol.2007.07.009
32. Santos F, Tafur JP, Abad J, Fernández Romero AJ (2019) Structural modifications and ionic transport of PVA-KOH hydrogels applied in Zn/Air batteries. J Electroanal Chem 850:113380. https://doi.org/10.1016/j.jelechem.2019.113380
33. Iles Velez AA, Tafur JP, Thibault T (2022) A dual theoretical and experimental approach. about Transporting Conduction Process on Chitosan / VAVTDFilms
34. Salehan SS, Nadirah BN, Saheed MSM et al (2021) Conductivity, structural and thermal properties of corn starch-lithium iodide nanocomposite polymer electrolyte incorporated with Al2O3. J Polym Res 28:1–11. https://doi.org/10.1007/S10965-021-02586-Y/METRICS
35. Hodge RM, Edward GH, Simon GP (1996) Water absorption and states of water in semicrystalline poly(vinyl alcohol) films. Polym (Guildf) 37:1371–1376. https://doi.org/10.1016/0032-3861(96)81134-7
36. Aziz SB, Hamsan MH, Kadir MFZ et al (2019) Development of polymer blend electrolyte membranes based on chitosan: Dextran with high ion transport properties for EDLC application. Int J Mol Sci 20:3369. https://doi.org/10.3390/ijms20133369
37. Tafur JP, Santos F, Fernández Romero AJ (2015) Influence of the ionic liquid type on the gel polymer electrolytes properties. Membr (Basel) 5:752–771. https://doi.org/10.3390/membranes5040752
38. Zhang J, Wang Y, Zhang L et al (2014) Understanding changes in cellulose crystalline structure of lignocellulosic biomass during ionic liquid pretreatment by XRD. Bioresour Technol 151:402–405. https://doi.org/10.1016/J.BIORTECH.2013.10.009
39. Sing Ngai K, Ramesh S, Ramesh K, Ching Juan J (2016) A review of polymer electrolytes: fundamental, approaches and applications. Ionics (Kiel) 22:1259–1279. https://doi.org/10.1007/S11581-016-1756-4
40. Abdullah OGH, Hanna RR, Salman YAK (2019) Structural and electrical conductivity of CH:MC bio-poly-blend films: optimize the perfect composition of the blend system. Bull Mater Sci 2019 422 42:64. https://doi.org/10.1007/S12034-019-1742-3
41. Yusof YM, Shukur MF, Illias HA, Kadir MFZ (2014) Conductivity and electrical properties of corn starch-chitosan blend biopolymer electrolyte incorporated with ammonium iodide. Phys Scr 89:035701. https://doi.org/10.1088/0031-8949/89/03/035701
42. Yusof YM, Illias HA, Shukur MF, Kadir MFZ (2017) Characterization of starch-chitosan blend-based electrolyte doped with ammonium iodide for application in proton batteries. Ionics (Kiel) 23:681–697. https://doi.org/10.1007/s11581-016-1856-1
43. Rokicki G, Kuran W (1984) Cyclic carbonates obtained by reactions of alkali metal carbonates with epihalohydrins. Bull Chem Soc Jpn 57:1662–1666. https://doi.org/10.1246/BCSJ.57.1662
44. Nusrath Unnisa C, Chitra S, Selvasekarapandian S et al (2018) Development of poly(glycerol suberate) polyester (PGS)–PVA blend polymer electrolytes with NH4SCN and its application. Ionics (Kiel) 24:1979–1993. https://doi.org/10.1007/s11581-018-2466-x
45. Tuhin MO, Rahman N, Haque ME et al (2012) Modification of mechanical and thermal property of chitosan–starch blend films. Radiat Phys Chem 81:1659–1668. https://doi.org/10.1016/j.radphyschem.2012.04.015
46. Rana VK, Pandey AK, Singh RP et al (2010) Enhancement of thermal stability and phase relaxation behavior of chitosan dissolved in aqueous l-lactic acid: using 'silver nanoparticles' as nano filler. Macromol Res 18:713–720. https://doi.org/10.1007/s13233-010-0801-9
47. Paulino AT, Simionato JI, Garcia JC, Nozaki J (2006) Characterization of chitosan and chitin produced from silkworm crysalides. Carbohydr Polym 64:98–103. https://doi.org/10.1016/j.carbpol.2005.10.032
48. Strydom CA, Collins AC, Bunt JR (2015) The influence of various potassium compound additions on the plasticity of a high-swelling south african coal under pyrolyzing conditions. J Anal Appl Pyrolysis 112:221–229. https://doi.org/10.1016/j.jaap.2015.01.023
49. Zhang P, Wang K, Pei P et al (2021) Selection of hydrogel electrolytes for flexible zinc–air batteries. Mater Today Chem 21:100538. https://doi.org/10.1016/j.mtchem.2021.100538
50. Hatta FF, Yahya MZA, Ali AMM et al (2005) Electrical conductivity studies on PVA/PVP-KOH alkaline solid polymer blend electrolyte. Ionics (Kiel) 11:418–422. https://doi.org/10.1007/BF02430259
51. Petrowsky M, Frech R (2010) Application of the compensated Arrhenius formalism to self-diffusion: implications for ionic conductivity and dielectric relaxation. J Phys Chem B 114:8600–8605. https://doi.org/10.1021/jp1020142
52. Cai M, Park S (1996) Spectroelectrochemical studies on dissolution and passivation of zinc electrodes in alkaline solutions. J Electrochem Soc 143:2125–2131. https://doi.org/10.1149/1.1836970
53. Hosseini S, Lao-atiman W, Jing Han S et al (2018) Discharge performance of zinc-air flow batteries under the effects of sodium dodecyl sulfate and pluronic F-127 OPEN. Sci Rep 8:14909. https://doi.org/10.1038/s41598-018-32806-3
54. Li Y, Fan X, Liu X et al (2019) Long-battery-life flexible zinc–air battery with near-neutral polymer electrolyte and nanoporous integrated air electrode. J Mater Chem A 7:25449–25457. https://doi.org/10.1039/C9TA09137H
55. Ng LS, Mohamad AA (2006) Protonic battery based on a plasticized chitosan-NH4NO3 solid polymer electrolyte. J Power Sources 163:382–385. https://doi.org/10.1016/j.jpowsour.2006.09.042
56. Jothi MA, Vanitha D, Sundaramahalingam K, Nallamuthu N (2022) Utilisation of corn starch in production of 'eco friendly' polymer electrolytes for proton battery applications. Int J Hydrogen Energy 47:28763–28772. https://doi.org/10.1016/j.ijhydene.2022.06.192
57. Song A, Huang Y, Zhong X et al (2017) Gel polymer electrolyte with high performances based on pure natural polymer matrix of potato starch composite lignocellulose. Electrochim Acta 245:981–992. https://doi.org/10.1016/j.electacta.2017.05.176
58. Mohamed AS, Shukur MF, Kadir MFZ, Yusof YM (2020) Ion conduction in chitosan-starch blend based polymer electrolyte with ammonium thiocyanate as charge provider. J Polym Res 27. https://doi.org/10.1007/S10965-020-02084-7